Nuclear Instruments and Methods in Physics Research A 768 (2014) 96–103

Contents lists available at ScienceDirect

Nuclear Instruments and Methods in Physics Research A

journal homepage: www.elsevier.com/locate/nima

Gain monitoring of telescope array photomultiplier cameras for the first 4 years of operation

B.K. Shin [d], H. Tokuno [c], Y. Tsunesada [c], T. Abu-Zayyad [a], R. Aida [b], M. Allen [a], R. Anderson [a], R. Azuma [c], E. Barcikowski [a], J.W. Belz [a], D.R. Bergman [a], S.A. Blake [a], R. Cady [a], B.G. Cheon [d], J. Chiba [e], M. Chikawa [f], E.J. Cho [d], W.R. Cho [g], H. Fujii [h], T. Fujii [i], T. Fukuda [c], M. Fukushima [j,t], W. Hanlon [a], K. Hayashi [c], Y. Hayashi [i], N. Hayashida [l], K. Hibino [l], K. Hiyama [j], K. Honda [b], T. Iguchi [c], D. Ikeda [j], K. Ikuta [b], N. Inoue [m], T. Ishii [b], R. Ishimori [c], D. Ivanov [a,n], S. Iwamoto [b], C.C.H. Jui [a], K. Kadota [o], F. Kakimoto [c], O. Kalashev [k], T. Kanbe [b], K. Kasahara [p], H. Kawai [q], S. Kawakami [i], S. Kawana [m], E. Kido [j], H.B. Kim [d], H.K. Kim [g], J.H. Kim [r], J.H. Kim [a], K. Kitamoto [f], S. Kitamura [c], Y. Kitamura [c], K. Kobayashi [e], Y. Kobayashi [c], Y. Kondo [j], K. Kuramoto [i], V. Kuzmin [k], Y.J. Kwon [g], S.I. Lim [s], S. Machida [c], K. Martens [t], J. Martineau [a], T. Matsuda [h], T. Matsuura [c], T. Matsuyama [i], J.N. Matthews [a], I. Myers [a], M. Minamino [i], K. Miyata [e], Y. Murano [c], K. Nagasawa [n], S. Nagataki [u], T. Nakamura [v], S.W. Nam [s], T. Nonaka [j], S. Ogio [i], M. Ohnishi [j], H. Ohoka [j], K. Oki [j], D. Oku [b], T. Okuda [i], A. Oshima [i], S. Ozawa [p], I. H. Park [s], M.S. Pshirkov [w], D.C. Rodriguez [a], S.Y. Roh [r], G. Rubtsov [k], D. Ryu [r], H. Sagawa [j], N. Sakurai [i], A.L. Sampson [a], L.M. Scott [n], P.D. Shah [a], F. Shibata [b], T. Shibata [j], H. Shimodaira [j], J.I. Shin [g], T. Shirahama [m], J.D. Smith [a], P. Sokolsky [a], T.J. Sonley [a], R.W. Springer [a], B. T. Stokes [a], S.R. Stratton [a,n], T. Stroman [a], S. Suzuki [h], Y. Takahashi [j], M. Takeda [j], A. Taketa [x], M. Takita [j], Y. Tameda [j], H. Tanaka [i], K. Tanaka [y], M. Tanaka [h], S.B. Thomas [a], G.B. Thomson [a], P. Tinyakov [k,v], I. Tkachev [k], T. Tomida [b], S. Troitsky [k], K. Tsutsumi [c], Y. Tsuyuguchi [b], Y. Uchihori [z], S. Udo [l], H. Ukai [b], G. Vasiloff [a], Y. Wada [m], T. Wong [a], M. Wood [a], Y. Yamakawa [j], R. Yamane [i], H. Yamaoka [h], K. Yamazaki [i], J. Yang [s], Y. Yoneda [i], S. Yoshida [q], H. Yoshii [aa], X. Zhou [f], R. Zollinger [a], Z. Zundel [a]

[a] University of Utah, High Energy Astrophysics Institute, Salt Lake City, UT, USA
[b] University of Yamanashi, Interdisciplinary Graduate School of Medicine and Engineering, Kofu, Yamanashi, Japan
[c] Tokyo Institute of Technology, Meguro, Tokyo, Japan
[d] Hanyang University, Seongdong-gu, Seoul, Republic of Korea
[e] Tokyo University of Science, Noda, Chiba, Japan
[f] Kinki University, Higashi Osaka, Osaka, Japan
[g] Yonsei University, Seodaemun-gu, Seoul, Republic of Korea
[h] Institute of Particle and Nuclear Studies, KEK, Tsukuba, Ibaraki, Japan
[i] Osaka City University, Osaka, Osaka, Japan
[j] Institute for Cosmic Ray Research, University of Tokyo, Kashiwa, Chiba, Japan
[k] Institute for Nuclear Research of the Russian Academy of Sciences, Moscow, Russia
[l] Kanagawa University, Yokohama, Kanagawa, Japan
[m] Saitama University, Saitama, Saitama, Japan
[n] Rutgers University, Piscataway, USA
[o] Tokyo City University, Setagaya-ku, Tokyo, Japan
[p] Waseda University, Advanced Research Institute for Science and Engineering, Shinjuku-ku, Tokyo, Japan
[q] Chiba University, Chiba, Chiba, Japan
[r] Department of Physics, School of Natural Sciences, Ulsan National Institute of Science and Technology, UNIST-gil, Ulsan, Republic of Korea
[s] Ewha Womans University, Seodaaemun-gu, Seoul, Republic of Korea
[t] Kavli Institute for the Physics and Mathematics of the Universe (WPI), Todai Institutes for Advanced Study, The University of Tokyo, Kashiwa, Chiba, Japan
[u] Kyoto University, Sakyo, Kyoto, Japan
[v] Kochi University, Kochi, Kochi, Japan
[w] University Libre de Bruxelles, Brussels, Belgium
[x] Earthquake Research Institute, University of Tokyo, Bunkyo-ku, Tokyo, Japan
[y] Hiroshima City University, Hiroshima, Hiroshima, Japan

[z] National Institute of Radiological Science, Chiba, Chiba, Japan
[aa] Ehime University, Matsuyama, Ehime, Japan

ARTICLE INFO

Article history:
Received 16 June 2014
Received in revised form
16 September 2014
Accepted 21 September 2014
Available online 2 October 2014

Keywords:
Ultra-high energy cosmic rays
Air fluorescence telescope
Calibration of photomultiplier

ABSTRACT

The stability of the gain of the photomultiplier (PMT) camera for the Fluorescence Detector (FD) of the Telescope Array experiment was monitored using an ^{241}Am loaded scintillator pulsers (YAP) and a diffused xenon flasher (TXF) for a selected set of 35 PMT-readout channels. From the monitoring of YAP pulses over four years of FD operation, we found slow monotonic drifts of PMT gains at a rate of $-1.7\sim+1.7$%/year. An average of the PMT gains over the 35 channels stayed nearly constant with a rate of change measured at -0.01 ± 0.31(stat)±0.21(sys)%/year. No systematic decrease of the PMT gain caused by the night sky background was observed. Monitoring by the TXF also tracked the PMT gain drift of the YAP at 0.88 ± 0.14(stat)%/year.

1. Introduction

The Telescope Array (TA) experiment is located in the western desert of Utah, USA, and has been observing ultra-high energy cosmic rays (UHECRs) in the northern hemisphere sky since 2007 [1]. The main goals of TA are to measure the energy spectrum, the mass composition, and the arrival direction anisotropy of UHECRs by detecting extensive air showers (EASs) initiated by primary cosmic rays with energies above $\sim10^{18}$ eV.

TA consists of two major components: A large-area surface detector (SD) array of plastic scintillation counters measures the lateral distribution of secondary particles on the ground, and three fluorescence detector (FD) stations track the longitudinal development of the EAS in the atmosphere. The SD array covers a total area of about 700 km^2 with 507 counters and operates with a duty factor in excess of 95% [2]. A total of 38 fluorescence telescopes are distributed over three stations (12–14 each) located at the periphery of the surface array, observing the atmospheric volume directly over the SD counters [3]. The FD achieves about 10% duty cycle, operating on clear, moonless nights.

The FD performs a calorimetric measurement of the primary energy of UHECRs by integrating the energy deposit by the EAS particles in the atmosphere. The FD also measures the depth of the shower maximum (X_{max}), which gives a statistical measure of the composition of the primary cosmic rays.

The FD stations are located at three sites, Middle Drum (MD), Black Rock Mesa (BRM), and Long Ridge (LR), each separated by about 30 km and forming a triangle around the SD array. The MD station comprises 2×7 refurbished HiRes-I telescopes [4]. The BRM and LR stations each consist of 2×6 newly designed telescopes. This paper describes the long-term gain monitoring of the FD cameras at the BRM and LR sites over four years from March 2008 to December 2011 using two kinds of light pulsers, YAP and Xenon. The night sky background (NSB) light was used to estimate the total exposure to the UV light of the PMTs during these four years.

2. FD Camera

Each FD telescope at the BRM and LR stations has a segmented spherical mirror of 3.3 m in diameter, and an imaging camera installed at the focal plane located 3.0 m in front of the mirror [3]. Each camera is composed of a matrix of 16×16 PMTs (Hamamatsu R9508) each with an ultraviolet (UV)-transparent acrylic front window. The front face of each PMT is covered with a UV band-pass filter (BG3, Schott AG), accepting the UV air fluorescence signal in the near-UV range, and blocking out the night sky background at visible wavelengths and in the far-UV and beyond. The rear side of the PMT is equipped with a High-Voltage (HV) divider chain and preamplifier assembly. The temperature in each camera box is measured by a thermistor probe (Nikkiso-Therm Co., Ltd., YSI44006).

FD observations occur only on clear moonless night and the accumulated observation time is approximately 12% of the total elapsed time. In order to minimize long-term degradation in PMT gain from non-reversible aging effects, all the PMTs are operated at a relatively low tube gain of $\sim6\times10^4$ in tandem with a preamplifier. The preamplifier output of each PMT is transmitted to a Signal Digitizer and Finder (SDF) module over a 25 m long twisted-pair cable. The SDF digitizes and records the signal waveform at a sampling rate of 10 MHz with 14-bits of dynamic range [5,6].

3. PMT calibration and monitoring

Three types of light sources are used for the calibration and monitoring of the camera PMTs at the BRM and LR stations. First, a standard pulsed UV light source, CRAYS (Calibration using RAYleigh Scattering), provides the initial calibration for each combination of PMT, preamplifier, and readout electronic channel. The CRAYS consists of a nitrogen laser and a gas-filled chamber in which laser-generated photons are Rayleigh-scattered by the molecules. The polarization of the laser was measured to be 4% and its effect on the scattering cross-section was corrected accordingly. Each PMT assembly is then calibrated using the light scattered at 90°. A total of 50 PMTs were calibrated by the CRAYS in the laboratory at the Institute for Cosmic Ray Research (ICRR), Japan [7]. Then they were transported to the TA experimental site in Utah, USA. Two CRAYS-calibrated PMTs were installed in each camera.[1] The first, which we call the standard PMT, is placed at the center of the camera, and the second PMT at a location near a corner of the camera. Gain accuracy of calibration by CRAYS at ICRR is 7.2%. After the transport of PMTs from the ICRR, along with the installation into the FD stations in the TA site, light yields of YAP loaded PMTs have been measured to be stable to within 3.7% [7].

Second, a diffused xenon flasher is installed at the center of each mirror, facing the camera. This device is referred to as a Telescope

E-mail addresses: bkshin@hanyang.ac.kr (B.K. Shin), bgcheon@hanyang.ac.kr (B.G. Cheon).

[1] Two cameras at the BRM site, #BRM00 and #BRM06 are each equipped with a third CRAYS-calibrated PMT.

http://dx.doi.org/10.1016/j.nima.2014.09.059
0168-9002/

Table 1
Summary of calibration and monitoring of the FD system.

Time	Calibration and monitoring
2007 Jun.	Start of the FD observation with preliminary gain (HV) settings
2008 Jan.	CRAYS calibration of 50 PMTs, and measurement of the YAP at ICRR, Japan
2008 Mar.	Installation of CRAYS-calibrated PMTs and measurement of the YAP
	HV adjustment for the gain setting of all PMTs using the TXF
	Measurement of the effect of multiple reflections with mirrors covered with black cloth during TXF mini-runs
2008 Oct.	Measurement of the effect of multiple reflections with mirrors covered with black cloth during the TXF mini-run
Obs. time	Routine monitoring by the YAP (100 pulses) and the TXF (10–20 shots) every hour during FD observation

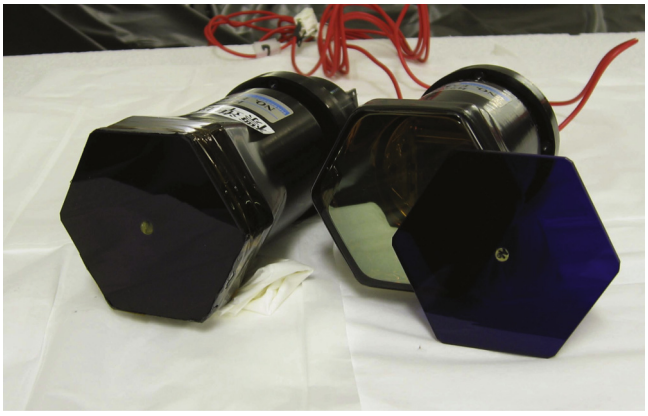

Fig. 1. Photograph of a PMT with YAP embedded in the BG3 filter [7].

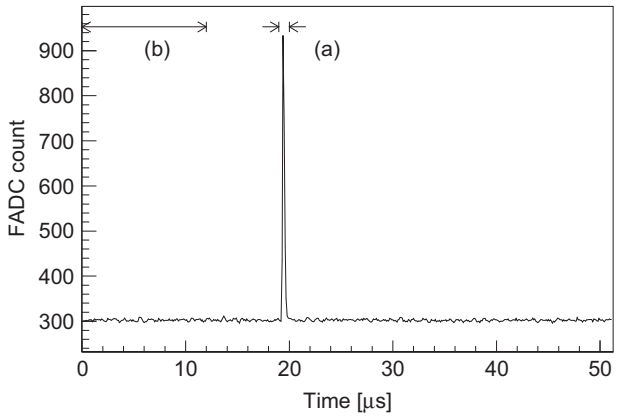

Fig. 2. Typical waveform recorded for YAP signals: (a) charge integration time range for the signal and (b) offset pedestal measurement time range.

Xenon Flasher (TXF) and provides the relative gain calibration among all the PMTs in a camera [9]. We equalized the gains within each camera by iteratively flashing the TXF and adjusting the HV such that the gain of each channel matches that of the standard PMT. The angular dependence of the illumination by the point-source TXF on the planar camera leads to a maximum of 5% difference in light flux on PMTs near the center from those along the edge. This effect was taken into account in the gain balancing. The mirror was covered with black cloth during the HV adjustment to block out the Fresnel-reflected photons from the camera box window and the BG3 filter and photo-cathode [8], which could come back to the mirror and reenter the PMT otherwise [9].

The initial HV values were set in March 2008 during the commissioning of the FD system; these values were kept for all the PMTs (6144 channels), except for those few PMTs which were replaced. Since that time, the TXFs have been used during observation for routine monitoring of the relative gains of the PMT-readout channels.

The gains of the CRAYS-calibrated PMTs have also been monitored using the YAP light source, which is installed in extrusions at the centers of the BG3 filter for those tubes [10,11]. A signal from an ^{241}Am α source has been recorded to perform the long-term gain monitoring of the PMT-readout channels during the subsequent four years of FD operation. A more detailed description of the YAP pulsers will be given in Section 3.1. A history of calibration and monitoring performed by these light sources is summarized in Table 1.

3.1. YAP pulser

The YAP pulser, shown in Fig. 1, contains a small piece of $YAlO_3$:Ce scintillator in an aluminum can (diameter 4 mm; height 1 mm). It is potted in an extrusion positioned at the center of the BG3 filter with epoxy glue (EPOXY TECHNOLOGY, EPO-TEK 305) together with a neutral density filter to adjust the light output. The YAP scintillator is loaded by a small amount of ^{241}Am α source and generates pulses of UV photons at wavelength $\sim$350 nm with width $\sim$40 ns, repeated at about 50 Hz. The temperature coefficient of the YAP light-yield is known to be small ($-0.23\%/^{\circ}$C) [12], and has a negligibly small effect on the long-term gain monitoring of the PMT-readout channels for the TA experiment.

During FD observation, camera data for 100 YAP shots were taken at the start of each hour. During these one-minute "YAP mini-runs", the SDF cards were switched to a dedicated single-pixel trigger mode (YAP mini-run). A typical YAP-induced waveform is shown in Fig. 2: the first quarter of waveform sampling window is the pedestal region, therefore the triggered signal is always placed after the first quarter [5].

In the YAP analysis, we integrate the signal region over 11 time bins (1.1 μs) around the signal peak. The DC offset, or pedestal, for each channel is calculated from the average of the first 120 time bins (12 μs) for each waveform, as shown in Fig. 2. The pedestal values are subtracted from the bin signals during the integration process. From the distribution of the integrated YAP signal obtained by an individual YAP mini-run, a mean value (S_{YAP}) and a standard deviation (σ_{YAP}) are determined.

Fig. 3 shows a history of S_{YAP} and σ_{YAP} values for one of the standard PMTs, placed in the #LR00 telescope, using data from $\sim$4200 YAP mini-runs collected between March 2008 and December 2011. A typical value of S_{YAP} is $\sim$970 FADC counts (measured at $\sim$25 °C), equivalent to $\sim$485 photo-electrons. The resolution ($=\sigma_{YAP}/S_{YAP}$) is measured to be about 7%.

Scatter-plots of S_{YAP} values with the measured temperature of the camera box for the standard PMT in the #LR00 telescope are shown in Fig. 4. Data from the four years are shown separately, each fitted to a different linear function. We obtained the slope to calculate a gain-temperature coefficient, and the χ^2/NDF to select a CRAYS-calibrated PMT with stable YAP: an examination of the S_{YAP} vs. temperature scatter-plot from all the CRAYS calibrated PMTs showed a sudden change of light yield at the level of $\sim$10% in a

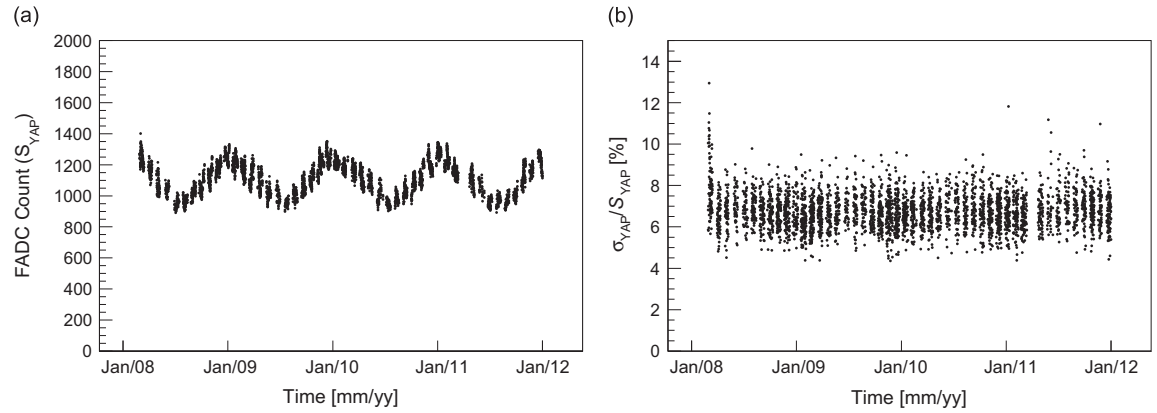

Fig. 3. History of (a) S_{YAP} and (b) σ_{YAP}/S_{YAP} for the standard PMT in the #LR00 telescope over four years. The S_{YAP} and σ denote the mean and standard deviation, respectively, obtained from the distribution of the integrated YAP signal for each YAP mini-run.

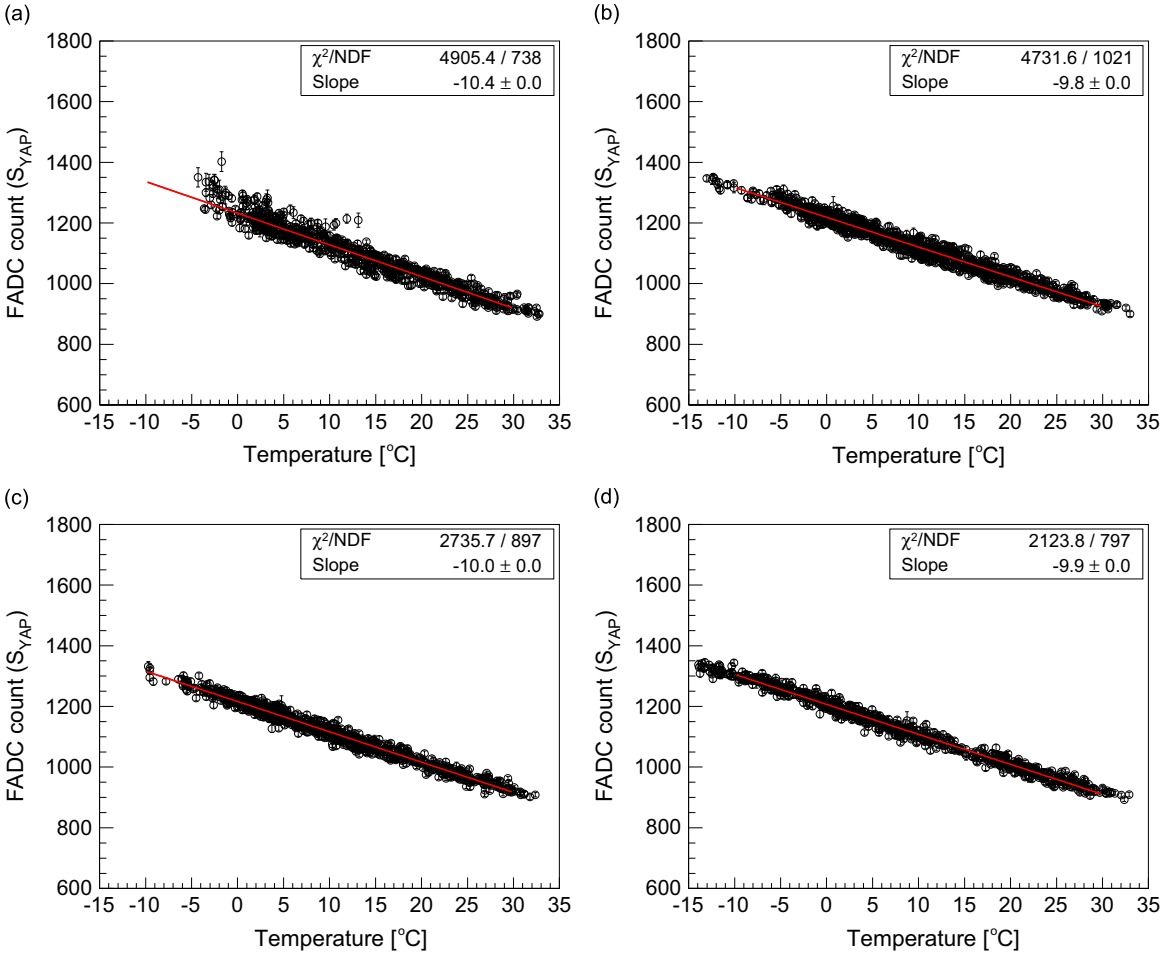

Fig. 4. Behavior of the YAP signals as a function of temperature of the camera in the #LR00 telescope over four years; (a) 2008, (b) 2009, (c) 2010, and (d) 2011.

number of unstable YAPs, causing large values of χ^2/NDF.[2] These PMT-readout channels out of the total 50 were set apart for further analysis. Only the 35 channels that were stable for at least three consecutive calendar years were retained for the studies described further on in this report. Fig. 5 shows the distribution of the fitted temperature coefficient for the 35 selected PMT-readout channels. The average temperature coefficients is -0.87 ± 0.09(stat)%/°C, which is consistent with the values measured on temperature range from -10 °C to 40 °C using 23 YAP-attached PMTs during initial laboratory tests in Japan [12]: -0.73%/°C for the PMT and preamplifier combined, and -0.23%/°C for the YAP light output at 24 °C.

In Fig. 6, we plot a subset of the S_{YAP} data from Fig. 3(a) using separate plotting symbols to differentiate the YAP data taken in seven temperature ranges at 5 °C (± 1°C) intervals with centers ranging from -5 °C to $+25$ °C. The plot demonstrates that the dominant time variation of S_{YAP} values is an oscillation correlated

[2] It is conceivable that temperature changes triggered a distortion of the scintillator membrane glued to the aluminum container and embedded in the BG3 filter by epoxy, thus affecting the light collection in the pulser.

to a yearly temperature cycle, and that the average S_{YAP} values within a given temperature range show a slow drift of the gain over four years. To quantify this slow drift, we made an individual fit to the S_{YAP} data for each of the five temperature ranges, for the 35 selected channels. We obtained an average gain slope (%/year change of S_{YAP} for four years) for each channel from the five separate fits for the different temperature ranges. The distributions of the mean slope and RMS variation for the 35 channels are given in Fig. 7. Fig. 7(a) shows a long-term gain change of the PMT-readout channels at a rate of -0.01 ± 0.31(stat)%/year. These values indicate that individual CRAYS-calibrated PMTs, together with their electronics, have a slow drift in their gain at the level of about ± 1.7%/year, but that the average gain of the 35 PMTs is constant at the level of -0.01 ± 0.31(stat) ± 0.21(sys)%/year. The systematic uncertainty of the gain slope is estimated by varying the selection cut of stable YAPs (0.14%/year) and from the RMS of the temperature slopes corresponding to different temperature ranges (0.16%/year) obtained from Fig. 7(b). In conclusion, we have observed no clear long-term degradation of the PMT gain over four years of the FD operation as described above, consistent with the result of accelerated laboratory measurement made by the manufacturer of which catalog for PMT fatigue measurement shows ~ 0 (± 10)% at 36 Coulomb.

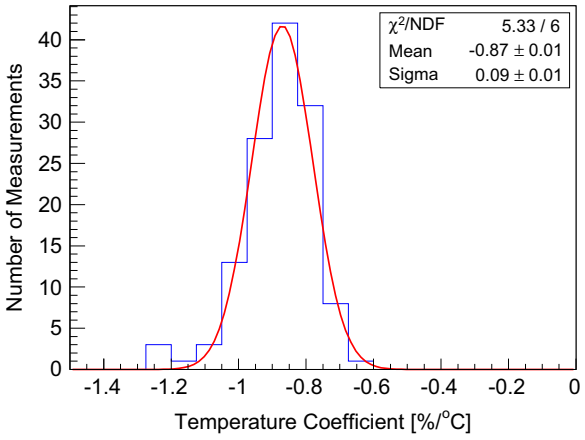

Fig. 5. Distribution of the fitted annual temperature coefficients for the 35 selected PMTs satisfying the condition of $\chi^2/\mathrm{NDF} < 10$, with the red line is gaussian fit. (For interpretation of the references to color in this figure caption, the reader is referred to the web version of this article.)

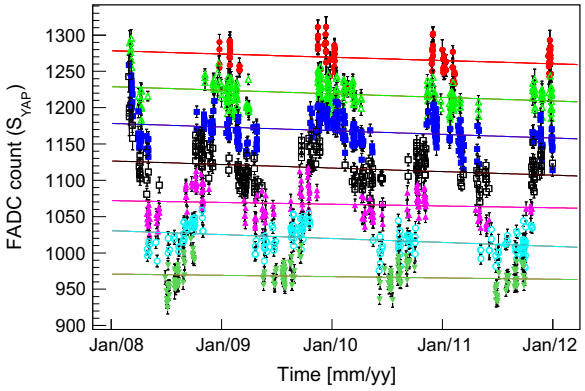

Fig. 6. Seasonal variation of the YAP signal for the standard PMT in the #LR00 telescope. The temperature ranges are color- and marker-coded, and results of linear fits over each temperature range, in 5 °C steps from −5 °C (top) to +25 °C (bottom), are also shown.

3.2. Telescope xenon flasher

The TXF consists of a Xenon flash lamp (Hamamatsu L4646) and a teflon diffuser of 4 mm thickness [9]. The TXF is mounted at the center of each mirror, and uniformly illuminates all 256 PMTs in each camera. The light intensity at the camera is equivalent to 2×10^4 p.e./PMT per shot. The typical pulse width is 2 μs FWHM emitted over a wide range of wavelengths between 200 and 2000 nm. Its shot-to-shot intensity fluctuation is ~1%.

The TXF data were taken in sequences of 10(20) events at the BRM(LR) station during normal FD observation. The TXF mini-runs are performed just after the YAP mini-run once every hour. A typical TXF signal is shown in Fig. 8. The waveforms are integrated for each TXF event after subtracting the DC offset. The integrated FADC count is corrected for differences in acceptance resulting from the small variation in the distance between TXF and each PMT that depends on its location off the optical axis. The signal size is also corrected for the multiple reflections between the PMT window and the mirror. The amount of additional light seen by each PMT is obtained by comparing the results measured with and without opaque black coverings on the mirrors. Fig. 9 shows the distribution of the ratios of the average signal areas taken (in March and October 2008) without covering over that with the mirrors covered. An average of the integrated signal for all the TXF events in one TXF mini-run (usually without mirror covering) corrected for multiple-reflections, is denoted as S_{TXF}. We define a relative gain, R_{TXF}, of each PMT-readout channel as follows:

$$R_{TXF} = S_{TXF}/A_{TXF} \quad (1)$$

where A_{TXF} is the average of S_{TXF} over 256 channels in one camera for each TXF mini-run.

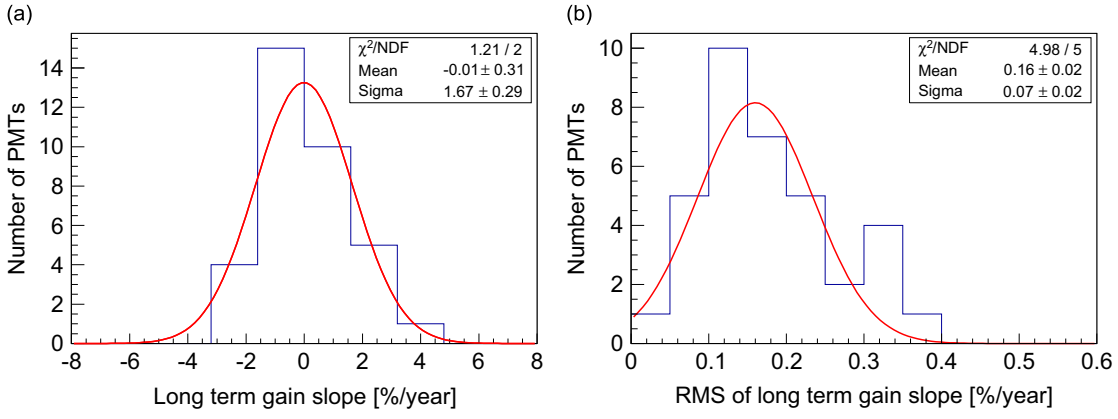

Fig. 7. Long-term behavior of (a) PMT gain slopes and (b) their RMS deviations for the 35 selected PMTs measured by the YAP. Each red line is a gaussian fit. (For interpretation of the references to color in this figure caption, the reader is referred to the web version of this article.)

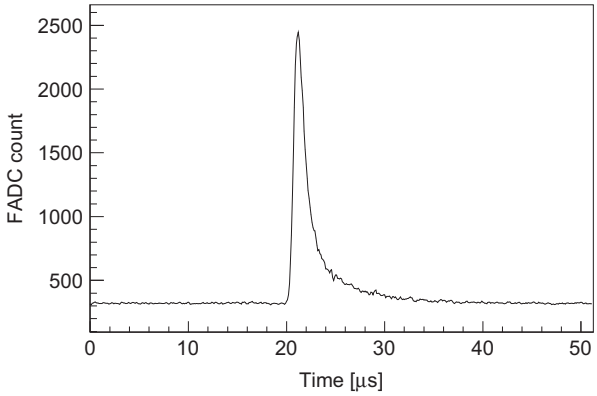

Fig. 8. Typical waveform recorded for diffused xenon flasher (TXF) signals.

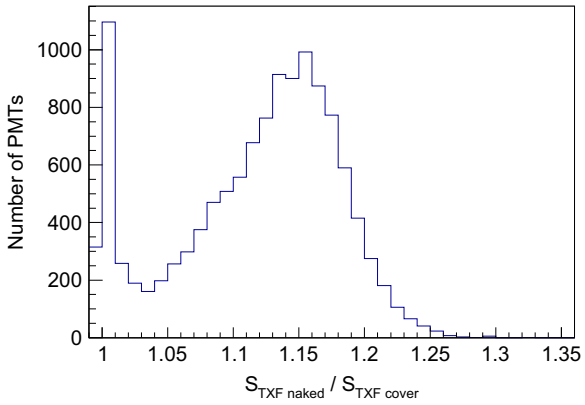

Fig. 9. Multiple reflection effect of all PMTs in BRM and LR station obtained by comparing the signal size with the mirrors covered with black cloth to that with the mirrors uncovered. The peak in the ratio at the value 1 is the case of central PMTs in each camera.

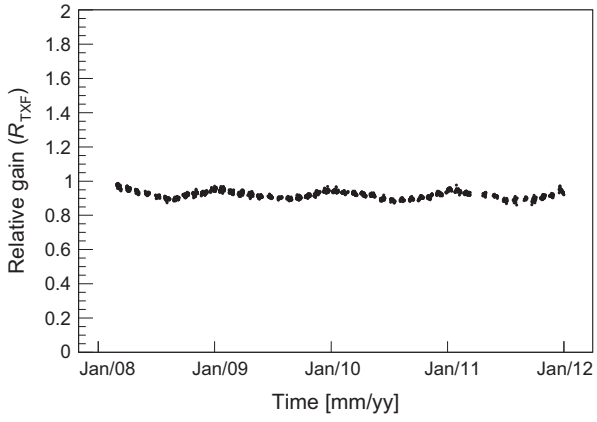

Fig. 10. History of R_{TXF} for the standard PMT in the #LR00 telescope.

The history of R_{TXF}, for the standard PMT in the #LR00 telescope, is plotted in Fig. 10 showing an oscillatory behavior correlated to the yearly temperature variation. The method of the gain slope measurement of R_{TXF} is the same as the case of S_{YAP}. The resulting gain slope determined for R_{TXF} is shown in Fig. 11.

The long term gain drift of the PMT readout channels is studied for both the YAP and TXF measurements. A channel-by-channel scatter-plot of the S_{YAP} slopes vs. R_{TXF} slopes is shown in Fig. 12(a) for the 35 selected PMTs. The distribution of the difference between the two slopes is shown in Fig. 12(b). The mean difference of the slopes is -0.32 ± 0.16(stat)%/year with an RMS of 0.88 ± 0.14(stat)%/year as shown in Fig. 12(b). The results show that the gain slopes

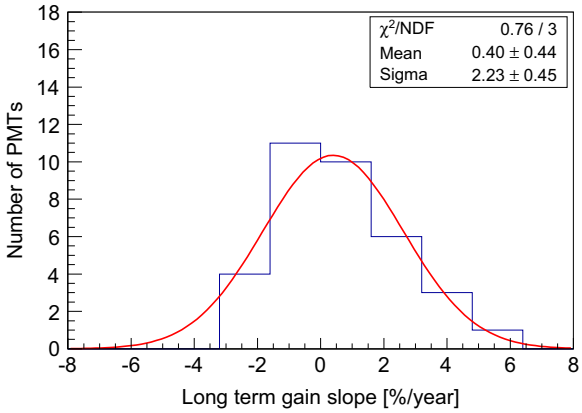

Fig. 11. Distribution of long-term gain slopes measured by the TXF, the red line being a gaussian fit. (For interpretation of the references to color in this figure caption, the reader is referred to the web version of this article.)

obtained using the YAP pulser and the TXF agree at the level of 0.88%/year or 3.5% over four years. The same level of agreement is demonstrated also in the RMS of 3.3% obtained for the double ratio of the slopes TXF/YAP measured in March 2008 and December 2011 as shown in Fig. 13. We assign 3.5% for the systematic uncertainty of the long-term gain monitoring using the YAP and TXF.

4. Estimate of exposure by night sky background

The PMTs of the FD telescopes are operated under "high dark current" conditions caused by the NSB. The level of NSB varies with time, location, and weather conditions of the FD measurement. In particular, the background light levels change when bright stars, other natural, and artificial light sources enter the field of view of each PMT.

The HV supplies for the PMTs are turned on 30 minutes before the start of observation each night. After a warm-up period, waveforms are recorded from two types of "pedestal mini-runs", one with telescope shutters closed and the second with the shutters open. During each pedestal mini-run, 1000 events are collected. The level of NSB is evaluated from the difference in pedestal levels obtained from the shutter-open and shutter-closed pedestal mini-runs. Fig. 14 shows a history of the NSB over four years of running where the average of the NSB over each month is plotted. In this figure, the error bars show the RMS variation of NSB. The variance of NSB in one pedestal run is consistent with the value expected from the NSB measured by the pedestal shift, when the contribution from the electronics noise observed in the pedestal mini-run is subtracted in quadrature, as shown in Fig. 15. The average of NSB over 50 CRAYS-calibrated PMTs is 10.0 photo-electrons/100 ns. The integrated flux of NSB, in the 290–430 nm window, received by the TA fluorescence telescope, is estimated to be 5.59×10^{11} [photons/(m^2 sr s)] at the elevation angle of $8^\circ \sim 25^\circ$ assuming 6.8 m^2 for the mirror collection area, 1.6×10^{-4} sr for the effective solid angle coverage of one PMT, and $\sim$16% for the averaged total optical efficiency of the camera.

With a PMT gain of 6×10^4, this amount of NSB corresponds to a dark current of 0.96 μA, and a total accumulated anode charge in one year operation of 3.6 Coulombs, assuming a duty factor of 12%.

5. Summary

The photo-sensors of TA's new FD are comprised of 6144 channels of PMT-readout in 24 telescopes at two FD stations. The 50 YAP-loaded PMT channels were calibrated by CRAYS at the ICRR, and the stability of the calibration was checked in situ at the

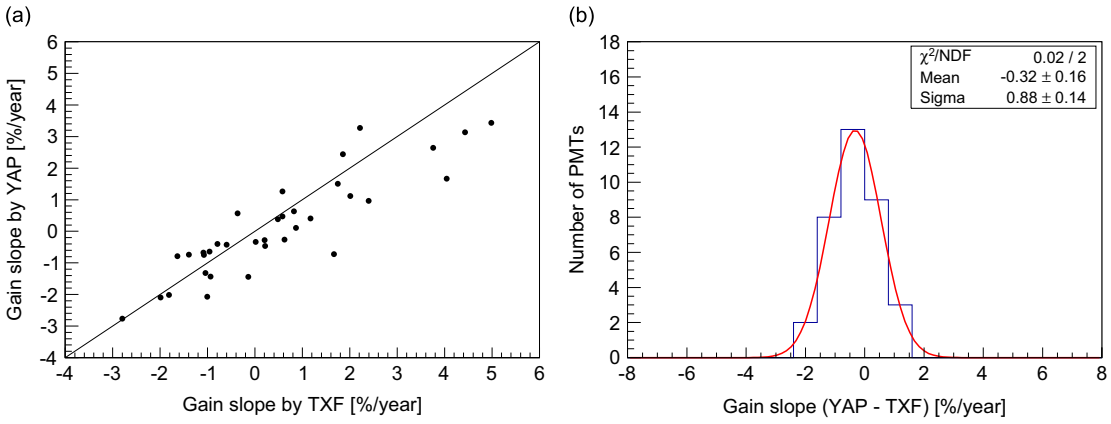

Fig. 12. (a) Scatter plot of long-term gain slopes obtained from the YAP vs. that obtained from the TXF and (b) difference of long-term gain slopes measured by the YAP and TXF, the red line being a gaussian fit. (For interpretation of the references to color in this figure caption, the reader is referred to the web version of this article.)

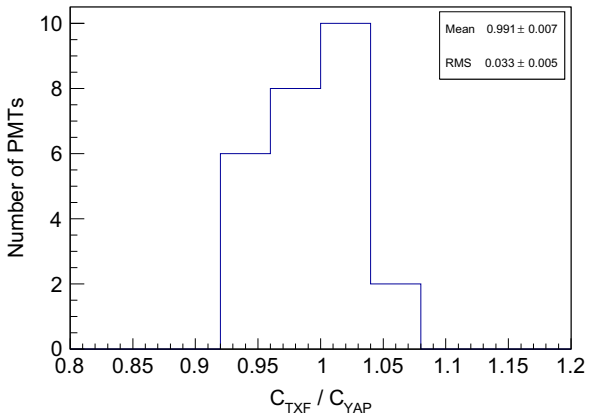

Fig. 13. Distribution of the C_{TXF}/C_{YAP} obtained from monthly data in March 2008 (A) and December 2011 (B). The definitions of C_{TXF} and C_{YAP} are $R_{TXF}(B)/R_{TXF}(A)$ and $S_{YAP}(B)/S_{YAP}(A)$, respectively.

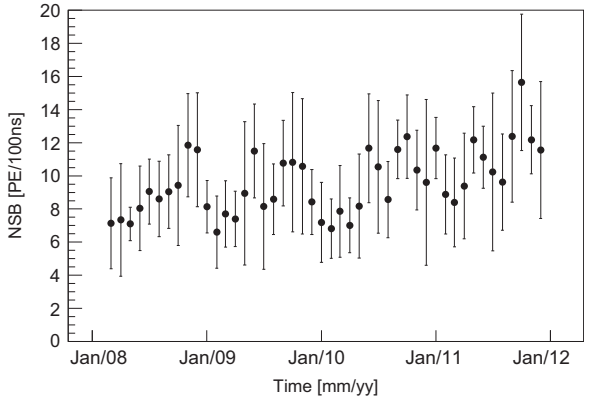

Fig. 14. History of NSB level over 4 years observed at the standard PMT in the #LR00 telescope. Each data point and its error bar indicate the mean and standard deviation from one month of data, respectively.

TA site [7]. Since the installation in March 2008, we have continuously monitored the variation in the gain of the CRAYS-calibration PMTs over four years using the YAP pulsers for 35 selected PMTs.

A slow monotonic drift of ± 1.7%/year was observed for these PMTs with a gain slope, averaged over the 35 selected PMT-readout channels of -0.01 ± 0.31(stat) $\pm$ 0.21(sys)%/year. No appreciable aging effect was observed at the PMT output charge accumulation rate of 3.6 Coulomb/year from the night sky background light. The gain slopes obtained independently by the TXF

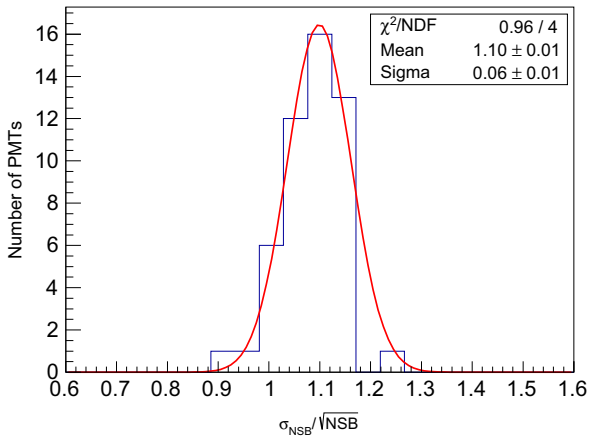

Fig. 15. Distribution of the standard deviation of NSB, the red line being a gaussian fit. (For interpretation of the references to color in this figure caption, the reader is referred to the web version of this article.)

Table 2
Overall gain accuracy of PMTs in FD cameras.

Item	Accuracy (%)
Initial calibration using CRAYS at ICRR [7]	7.2
Stability of calibration at TA on-site [7]	3.7
Long term stability over 4 years [This paper]	3.5
Total	8.8

agreed with the slopes measured by the YAP pulser with an accuracy of 3.5% for four years. The overall gain accuracy of the PMT in FD camera was estimated to be 8.8% from all the above items as summarized in Table 2.

Acknowledgments

We gratefully acknowledge Dr. M. Korjik and Prof. M. Kobayashi for elucidating discussions on the construction of the YAP pulser and its performance. The Telescope Array experiment is supported by the Japan Society for the Promotion of Science through Grants-in-Aid for Scientific Research on Specially Promoted Research (21000002) "Extreme Phenomena in the Universe Explored by Highest Energy Cosmic Rays", and the Inter-University Research Program of the Institute for Cosmic Ray Research; by the U.S. National Science Foundation awards PHY-0307098, PHY-0601915, PHY-0703893, PHY-0758342, and PHY-0848320 (Utah) and PHY-0649681 (Rutgers); by

the National Research Foundation of Korea (2006-0050031, 2007-0056005, 2007-0093860, 2010-0028071, 2013004883); by the Russian Academy of Sciences, RFBR grants 10-02-01406a and 11-02-01528a (INR), IISN project No. 4.4509.10 and Belgian Science Policy under IUAP VI/11 (ULB). The foundations of Dr. Ezekiel R. and Edna Wattis Dumke, Willard L. Eccles and the George S. and Dolores Dore Eccles all helped with generous donations. The State of Utah supported the project through its Economic Development Board, and the University of Utah through the Office of the Vice President for Research. The experimental site became available through the cooperation of the Utah School and Institutional Trust Lands Administration (SITLA), U.S. Bureau of Land Management and the U.S. Air Force. We also wish to thank the people and the officials of Millard County, Utah, for their steadfast and warm support. We gratefully acknowledge the contributions from the technical staffs of our home institutions and the University of Utah Center for High Performance Computing (CHPC). This work was partially supported by the Research Fund of Hanyang University (HY-2009-O).

References

[1] H. Sagawa, for the TA Collaboration, in: Proceedings of the 31st International Cosmic Ray Conference (ICRC), Łódź, Poland, 2009; Y. Tsunesada for the TA Collaboration, in: Proceedings of the 32nd ICRC, Beijing, 2011.
[2] T. Abu-Zayyad, et al., Nuclear Instruments and Methods in Physics Research Section A 689 (2012) 87.
[3] H. Tokuno, et al., Nuclear Instruments and Methods in Physics Research Section A 676 (2012) 54.
[4] T. Abu-Zayyad, et al., Nuclear Instruments and Methods in Physics Research Section A 450 (2000) 253.
[5] Y. Tameda, et al., Nuclear Instruments and Methods in Physics Research Section A 609 (2009) 364.
[6] A. Taketa, et al., Proceedings of the 29th ICRC 8 (2005) 209.
[7] S. Kawana, et al., Nuclear Instruments and Methods in Physics Research Section A 681 (2012) 68.
[8] D. Motta, S. Schönert, Nuclear Instruments and Methods in Physics Research Section A 539 (2005) 217.
[9] H. Tokuno, et al., Nuclear Instruments and Methods in Physics Research Section A 601 (2009) 364.
[10] M. Kobayashi, et al., Nuclear Instruments and Methods in Physics Research Section A 337 (1994) 355.
[11] V.A. Kachanov, et al., Nuclear Instruments and Methods in Physics Research Section A 314 (1992) 215.
[12] S. Ogio, et al., Nuclear Instruments and Methods in Physics Research Section A, to be submitted; Proceedings of the 31st ICRC, Łódź, Poland, 2009.